Journal of Magnetic Resonance 207 (2010) 114–123

Contents lists available at ScienceDirect

Journal of Magnetic Resonance

journal homepage: www.elsevier.com/locate/jmr

Cooperative pulses

Michael Braun, Steffen J. Glaser *

Department of Chemistry, Technische Universität München, 85747 Garching, Germany

ARTICLE INFO

Article history:
Received 31 May 2010
Revised 5 August 2010
Available online 25 August 2010

Keywords:
Optimal control theory
GRAPE algorithm
Phase cycles
Composite pulses
Shaped pulses
Difference spectroscopy

ABSTRACT

We introduce the concept of cooperative (COOP) pulses which are designed to compensate each other's imperfections. In multi-scan experiments, COOP pulses can cancel undesired signal contributions, complementing and generalizing phase cycles. COOP pulses can be efficiently optimized using an extended version of the optimal-control-based gradient ascent pulse engineering (GRAPE) algorithm. The advantage of the COOP approach is experimentally demonstrated for broadband and band-selective pulses.

1. Introduction

In addition to simple rectangular radio-frequency (rf) pulses with constant amplitudes and phases, composite and shaped pulses [1–4] are powerful tools for the manipulaton of spins in modern NMR spectroscopy and imaging. In practice, both composite and shaped pulses are implemented as a sequence of rectangular pulses (with different amplitudes and phases) and in the following, we will use the generic term "pulse" for both composite or shaped pulses. Only recently has it become possible to explore the physical limits of pulse performance [5–7] using methods from optimal control theory [8]. For example, for a given maximum rf amplitude and a desired bandwidth and robustness with respect to rf inhomogeneity, there exists a minimum pulse duration T^* that is required to achieve a desired average fidelity or performance index. It is not possible for a pulse to compensate *its own* imperfections to the desired degree if the pulse duration is shorter than T^*. Here, we show that pulse durations can be further reduced by allowing pulses to compensate *each others* imperfections. We refer to this class of *coop*eratively acting pulses as COOP pulses. In multi-scan experiments, for example, imperfections in individual scans are irrelevant if these imperfections cancel in the total accumulated signal. In many multi-scan experiments, phase cycles [9–12] are routinely used for the suppression of artifacts or unwanted signals: In each scan, a sequence of identical pulses is repeated, except for a systematic phase variation of the pulses (and the receiver). Here, we demonstrate that it is possible to improve the performance of pulse sequences by not only changing the overall phase of a given pulse in subsequent scans, but by cycling through a set of carefully designed COOP pulses which are in general not identical. Highly compensating COOP cycles can be efficiently optimized using an adapted version of the optimal-control-based gradient ascent pulse engineering (GRAPE) algorithm [13,14].

2. Theory

2.1. Single pulse optimization

Before describing the algorithm for the simultaneous optimization of a set of COOP pulses, we briefly review the standard optimal-control-based gradient ascent algorithm for the optimization of a single (shaped or composite) pulse.

Suppose for a given initial magnetization vector $\boldsymbol{M}(0)$ we want to find a pulse of duration T that optimizes a defined performance index or quality factor Φ, which depends only on the final magnetization vector $\boldsymbol{M}(T)$. In the case of an excitation pulse, for example, we start with z magnetization, i.e. $\boldsymbol{M}(0) = (0,0,1)^t$, and a simple quality factor could be defined as the x component of the final magnetization [16]. A given pulse is fully characterized by the time-dependent x and y components $v_x(t) = -\gamma B_{rf,x}(t)/2\pi$ and $v_y(t) = -\gamma B_{rf,y}(t)/2\pi$ (or alternatively by the total rf amplitude $v_{rf}(t) = \sqrt{v_x^2(t) + v_y^2(t)}$ and rf phase $\varphi(t) = \tan^{-1}\{v_y(t))/v_x(t)\}$.

We can improve the pulse if we know how the quality factor Φ responds when the controls $v_x(t)$ and $v_y(t)$ are varied, i.e. if we know the gradients $\delta\Phi/\delta v_x(t)$ and $\delta\Phi/\delta v_y(t)$. These gradients can be approximated using finite differences.

* Corresponding author. Fax: +49 89 289 13319.
E-mail address: Glaser@ch.tum.de (S.J. Glaser).

1090-7807/$ - see front matter © 2010 Elsevier Inc. All rights reserved.
doi:10.1016/j.jmr.2010.08.013

The same high-dimensional gradients $\delta\Phi/\delta v_x(t)$ and $\delta\Phi/\delta v_y(t)$ can efficiently be calculated to first order based on principles of optimal control theory [8,13–16]. This approach requires calculation of the trajectories of the magnetization vector $\boldsymbol{M}(t)$, and of the so-called costate vector $\boldsymbol{\lambda}(t)$, for $0 \leqslant t \leqslant T$ [8,13–21]. The desired gradients are approximated to first order by the x and y components of the cross product $\boldsymbol{M}(t) \times \boldsymbol{\lambda}(t)$ [16–18]:

$$\frac{\delta\Phi}{\delta v_x(t)} = M_y(t)\lambda_z(t) - M_z(t)\lambda_y(t), \tag{1}$$

$$\frac{\delta\Phi}{\delta v_y(t)} = M_z(t)\lambda_x(t) - M_x(t)\lambda_z(t). \tag{2}$$

For a spin with offset v_{off}, the effective field vector $v_e(t)$ is defined as

$$\boldsymbol{v}_e(t) = (v_x(t), v_y(t), v_{off})^t, \tag{3}$$

and starting from the initial magnetization vector $\boldsymbol{M}(0) = \boldsymbol{M}_i$, the trajectory of the magnetization vector $\boldsymbol{M}(t)$ can be calculated by solving the Bloch equations

$$\dot{\boldsymbol{M}}(t) = 2\pi\boldsymbol{v}_e(t) \times \boldsymbol{M}(t). \tag{4}$$

Here, for simplicity we assume that relaxation effects can be neglected, however if necessary they can be taken into account in a straightforward way [13,21].

If the pulse performance Φ depends only on the magnetization vector $\boldsymbol{M}(T)$ at the end of the pulse, the costate vector $\boldsymbol{\lambda}(T)$ is given by $\partial\Phi/\partial\boldsymbol{M}(T)$ [16], i.e. the three components of the costate vector $\boldsymbol{\lambda}(T) = (\lambda_x(T), \lambda_y(T), \lambda_z(T))^t$ are

$$\lambda_x(T) = \frac{\partial\Phi}{\partial M_x(T)}, \quad \lambda_y(T) = \frac{\partial\Phi}{\partial M_y(T)}, \quad \lambda_z(T) = \frac{\partial\Phi}{\partial M_z(T)}. \tag{5}$$

For example, if the quality factor is simply the projection of the final magnetization vector onto a desired target state $\boldsymbol{F}$, i.e.

$$\Phi_a = M_x(T)F_x + M_y(T)F_y + M_z(T)F_z, \tag{6}$$

the final costate vector is simply $\boldsymbol{\lambda}(T) = \boldsymbol{F}$ [16]. On the other hand, if the quality to reach a target state $\boldsymbol{F}$ is defined as [18]

$$\Phi_b = 1 - a_1(M_x(T) - F_x)^2 - a_2(M_y(T) - F_y)^2 - a_3(M_z(T) - F_z)^2, \tag{7}$$

the resulting final costate vector is given by $\boldsymbol{\lambda}(T) = -(2a_1(M_x - F_x), 2a_2(M_y - F_y), 2a_3(M_z - F_z))^t$. Here a_1, a_2 and a_3 represent the relative weights given to the desired match of the x, y, and z components of the magnetization vector and the target state.

The equation of motion for the costate vector has the same form as the Bloch equations (c.f. Eq. (4)) [16–18,21], i.e.

$$\dot{\boldsymbol{\lambda}}(t) = 2\pi\boldsymbol{v}_e(t) \times \boldsymbol{\lambda}(t), \tag{8}$$

and by propagating $\boldsymbol{\lambda}(T)$ backward in time, we obtain $\boldsymbol{\lambda}(t)$ for $0 \leqslant t \leqslant T$.

Robustness with respect to offset and rf inhomogeneity can be achieved by averaging the gradients over all offsets v_{off} and rf scaling factors s of interest [13,16]. Starting from an initial pulse with rf amplitudes $v_x(t)$ and $v_y(t)$, the pulse performance can be optimized by following this averaged gradient. In the simplest approach, the gradient information can be used in steepest ascent algorithms, but faster convergence can often be found using conjugate gradient or efficient quasi-Newton methods [22] that are also based on the gradients $\delta\Phi/\delta v_x(t)$ and $\delta\Phi/\delta v_y(t)$.

2.2. Optimization of COOP pulses

Now we consider a set of N individual pulses $P^{(j)}$ of duration T with rf amplitudes $v_x^{(j)}(t)$ and $v_y^{(j)}(t)$ for $j \in \{1,2,\ldots,N\}$. For a given initial state $\boldsymbol{M}^{(1)}(0) = \boldsymbol{M}^{(2)}(0) = \cdots = \boldsymbol{M}^{(N)}(0) = \boldsymbol{M}_i$, the corresponding N trajectories $\boldsymbol{M}^{(j)}(t)$ of the magnetization vectors under the pulses $P^{(j)}$ can be calculated for $0 \leqslant t \leqslant T$ using the Bloch equations. If the quality factor Φ depends only on the final magnetization vectors $\boldsymbol{M}^{(j)}(T)$, the components of the costate vectors $\boldsymbol{\lambda}^{(j)}(T)$ are given by

$$\lambda_x^{(j)}(T) = \frac{\partial\Phi}{\partial M_x^{(j)}(T)}, \quad \lambda_y^{(j)}(T) = \frac{\partial\Phi}{\partial M_y^{(j)}(T)}, \quad \lambda_z^{(j)}(T) = \frac{\partial\Phi}{\partial M_z^{(j)}(T)} \tag{9}$$

and the N trajectories $\boldsymbol{\lambda}^{(j)}(t)$ can be calculated for $0 \leqslant t \leqslant T$ using the equation of motion of the costate vectors in analogy to Eq. (8). The gradient of the quality factor Φ with respect to the controls $v_x^{(j)}(t)$ and $v_y^{(j)}(t)$ is given by the x and y components of the vectors $\boldsymbol{M}^{(j)}(t) \times \boldsymbol{\lambda}^{(j)}(t)$ [16]:

$$\frac{\delta\Phi}{\delta v_x^{(j)}(t)} = M_y^{(j)}(t)\lambda_z^{(j)}(t) - M_z^{(j)}(t)\lambda_y^{(j)}(t), \tag{10}$$

$$\frac{\delta\Phi}{\delta v_y^{(j)}(t)} = M_z^{(j)}(t)\lambda_x^{(j)}(t) - M_x^{(j)}(t)\lambda_z^{(j)}(t). \tag{11}$$

For example, consider the optimization of COOP excitation pulses with minimal overall phase error. If applied in successive scans, the real and imaginary parts of the accumulated signal $S_x + iS_y$ are proportional to the x and y components of the average magnetization vector

$$\overline{\boldsymbol{M}}(T) = \frac{1}{N}\sum_{j=1}^{N}\boldsymbol{M}^{(j)}(T). \tag{12}$$

The goal is to maximize $\overline{M}_x(T)$ and to minimize $\overline{M}_y(T)$ in order to minimize the phase error of the accumulated signal, while $\overline{M}_z(T)$ is irrelevant. This goal can be quantified by

$$\Phi_c = 1 - (1 - \overline{M}_x(T))^2 - a\overline{M}_y(T)^2, \tag{13}$$

which is a generalization of the quality factor Φ_b (c.f. Eq. (7)), where $\boldsymbol{M}(T)$ is replaced by $\overline{\boldsymbol{M}}(T)$, with $\boldsymbol{F} = (1,0,0)^t$, $a_1 = 1$, $a_2 = a$, and $a_3 = 0$. Here, the relative weight given to the deviation of $\overline{M}_x(T)$ and $\overline{M}_y(T)$ from the target values $F_x = 1$ and $F_y = 0$ can be adjusted by the parameter a. According to Eq. (9), the costate vectors $\boldsymbol{\lambda}^{(j)}(T)$ are given by

$$\boldsymbol{\lambda}^{(j)}(T) = \frac{2}{N}(1 - \overline{M}_x(T), -a\overline{M}_y(T), 0)^t, \tag{14}$$

which is independent of j, i.e. all costate vectors are identical at the end of the pulse ($\boldsymbol{\lambda}^{(1)}(T) = \boldsymbol{\lambda}^{(2)}(T) = \cdots = \boldsymbol{\lambda}^{(N)}(T)$) and depend on the average magnetization vector $\overline{\boldsymbol{M}}(T)$. However, the back propagation of the costates under the different pulses $P^{(j)}$ results in different trajectories $\boldsymbol{\lambda}^{(j)}(t)$ for $0 \leqslant t < T$.

With the trajectories $\boldsymbol{M}^{(j)}(t)$ and $\boldsymbol{\lambda}^{(j)}(t)$, the gradients (10), (11) can be efficiently calculated, providing a powerful means for the simultaneous optimization of a set of mutually compensating COOP pulses. In the following, illustrative examples will be given, to demonstrate the COOP approach. Experiments were performed on Bruker AV 250 and AV III 600 spectrometers using a sample of ≈1% H_2O in D_2O doped with copper sulfate.

3. Examples

3.1. Total elimination of magnetization

As a first illustrative example, we consider the problem of completely eliminating *all* components of the average magnetization vector, i.e. $\overline{M}_x(T) = \overline{M}_y(T) = \overline{M}_z(T) = 0$ in the absence of B_0 gradients, B_1 inhomogeneity and relaxation effects, starting from z magnetization Clearly, this cannot be accomplished by a single pulse and at least two scans are required to achieve this goal. We optimized COOP cycles consisting of two or three individual pulses, using the quality factor

$$\Phi_{elim} = 1 - \overline{M}_x(T)^2 - \overline{M}_y(T)^2 - \overline{M}_z(T)^2. \quad (15)$$

For the simplest case of a single spin on resonance, the extended GRAPE algorithm finds the intuitive solution of two rectangular 90° pulses with a relative phase shift of 180°. Similarly, the optimization of a three-step COOP cycle yields three 90° pulses with phase differences of 120° and 240° as expected (data not shown), demonstrating that the algorithm is able to "rediscover" simple phase cycles. If the elimination of magnetization is desired not only for the on-resonance case but for a finite range of offsets and limited rf amplitudes, the optimal solution is not clear *a priori*. For an offset range of ±10 kHz and a maximum rf amplitude of 10 kHz we optimized a two-step COOP cycle, consisting of two individual pulses with a duration of 50 μs each. For each individual pulse a different random pulse shape was created at the start of the optimization and no symmetry constraints were imposed. Fig. 1 shows the optimized pulse shapes, the final magnetization components after each individual pulse and the components of the average final magnetization vector as a function of offset. The two-step COOP cycle efficiently eliminates the average magnetization vector as expected. Here the optimal solution consists of two saturation pulses that are identical up to an overall phase shift of 180°. Each individual saturation pulse brings the magnetization vector to the transverse plane and hence eliminates the z component in each scan with high fidelity for the desired range of offsets. The remaining transverse magnetization components are then averaged to zero by repeating the saturation pulse with a phase shift of 180°. This solution is not unexpected and a single saturation pulse could have been optimized and phase cycled with the same result. However, initially it was by no means clear if this is in fact the best possible strategy. As the COOP approach is not limited to a restricted set of solutions (e.g. pairs of saturation pulses), it is also able to find unexpected solutions if they exist, as will be shown in the next examples.

3.2. Band-selective excitation pulses

As a second example, we consider band-selective COOP pulses that excite magnetization in a defined offset range and simultaneously eliminate the average magnetization vector in other offset ranges. We use the quality factor Φ_b (Eq. (7)) for various offset-dependent target states $\boldsymbol{F}(\nu_{off})$. Here we consider the example where $\boldsymbol{F}(\nu_{off}) = (1,0,0)^t$ for $|\nu_{off}| \leqslant 2$ kHz (the "pass band") and $\boldsymbol{F}(\nu_{off}) = (0,0,0)^t$ for 2 kHz $< |\nu_{off}| \leqslant 10$ kHz (the "stop band"). The pulse duration T and the maximum rf amplitude ν_{rf}^{max} were set to 500 μs and 10 kHz, respectively. In contrast to the first example, in this case the COOP optimization yields two different pulses that are not simply related by an overall phase shift (Fig. 2). Fig. 2 also shows the simulated and experimental final magnetization components created by the individual pulses and the average magnetization vector. While the response of the individual COOP pulses appears to be erratic, the cancellation of the undesired terms is almost perfect. An excellent match is found between experimental (gray) and simulated (black) data.

For comparison, Fig. 3 shows the results of a conventional approach based on two individually optimized pulses: a broadband pulse with a target state $\boldsymbol{F}_1(\nu_{off}) = (1,0,0)^t$ for $|\nu_{off}| \leqslant 10$ kHz and a band-selective pulse with $\boldsymbol{F}_2(\nu_{off}) = (1,0,0)^t$ for $|\nu_{off}| \leqslant 2$ kHz and $\boldsymbol{F}_2(\nu_{off}) = (-1,0,0)^t$ for 2 kHz $|\nu_{off}| \leqslant 10$ kHz. These pulses also yield the desired average magnetization profile. Very good suppression of the x component is achieved by this approach in the stop band. However, large residual y and z components of the average magnetization vector of more than 40% remain in the vicinity of the transition regions at ±2 kHz (see Fig. 3). In contrast, using the the COOP approach, the undesired y and z components can be almost completely suppressed in the pass band, the stop band as well as in the transition region (c.f. Fig. 2).

Similar results were found for band-selective inversion pulses and different ranges of pass and stop bands (data not shown). It is interesting to note that in the case of band-selective inversion (and complete elimination of the average magnetization vector in the stop band), the COOP approach resulted in two very similar pulses with a relative phase shift of 180°. In this case, the target profile of the average magnetization vector can be approached by a pulse that inverts the magnetization in the pass band and brings it into the transverse plane in the stop band. By repeating the pulse with a phase shift of 180°, all transverse magnetization components are perfectly cancelled. Hence in this case, the COOP approach yields a solution that could also be constructed using a conventional optimization of a single pulse combined with a phase cycle. However, it was by no means obvious before that this

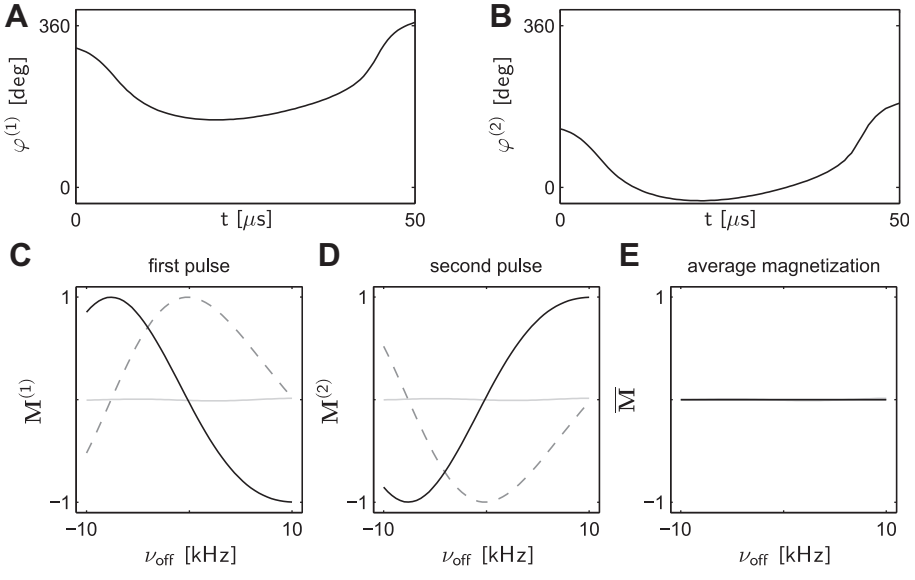

Fig. 1. Two-step COOP cycle for the complete elimination of the average magnetization vector $\overline{\boldsymbol{M}}$ for offsets in the range of ±10 kHz for a constant rf amplitude $\nu_{rf} = 10$ kHz and a pulse duration of 50 μs. A and B show the phase modulations $\varphi^{(1)}(t)$ and $\varphi^{(2)}(t)$, simulated offset-profiles of $\boldsymbol{M}^{(1)}(T)$, $\boldsymbol{M}^{(2)}(T)$ and $\overline{\boldsymbol{M}}(T)$ are drawn in C, D and E. The x, y and z components are plotted as solid black, dashed gray and solid gray curves, respectively.

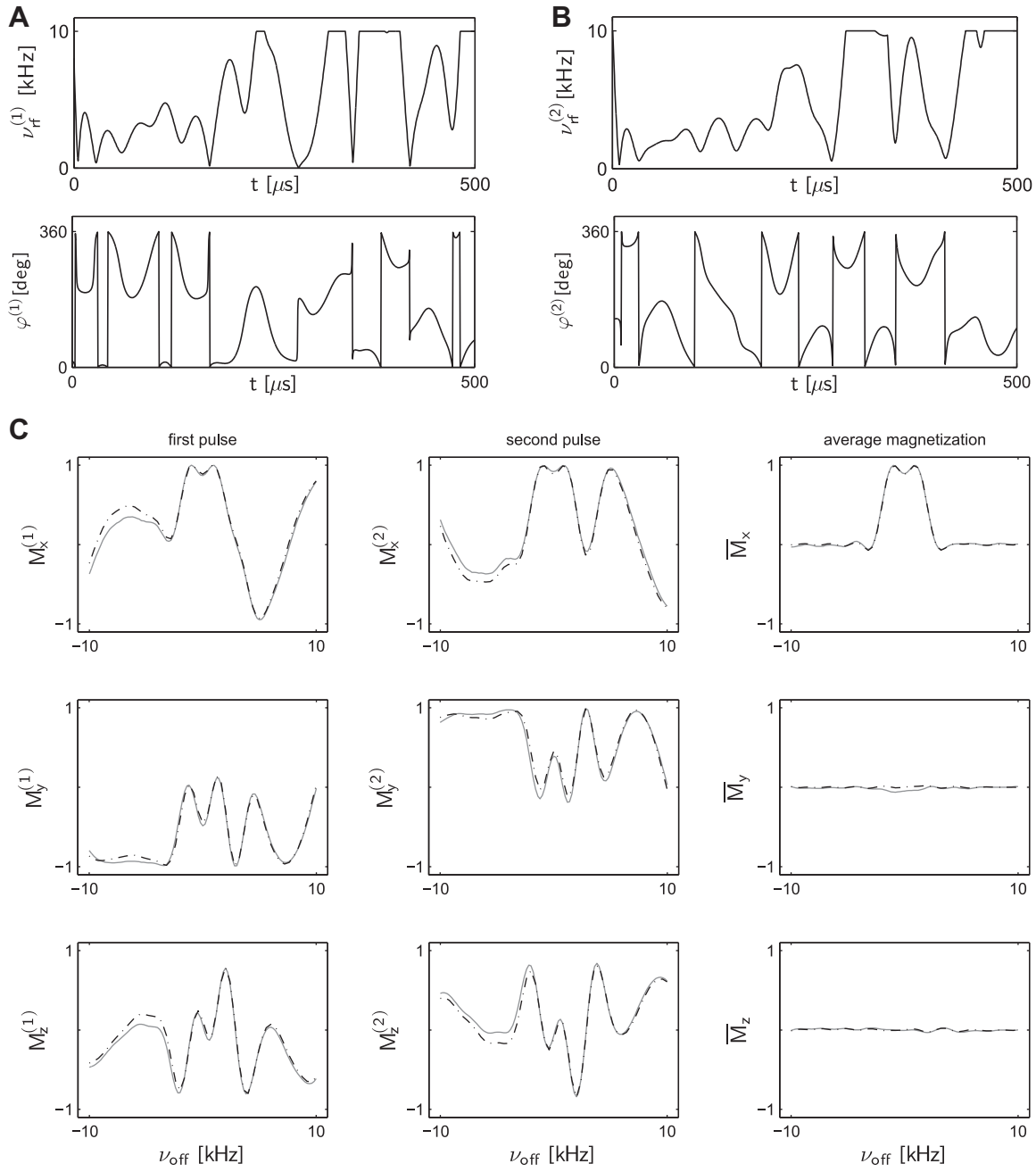

Fig. 2. Two-step COOP cycle for band-selective excitation and saturation. The rf amplitudes $\nu_{rf}^{(j)}(t)$ and phases $\varphi^{(j)}(t)$ for the two COOP pulses are shown in A and B. Simulated (black, dash-dotted curves) and experimental (gray, solid curves) components of $\boldsymbol{M}^{(1)}(T)$, $\boldsymbol{M}^{(2)}(T)$ and $\overline{\boldsymbol{M}}(\boldsymbol{T})$ are shown in C.

approach yields the optimal solution, which is in fact very different from the naive approach of combining individually optimized pulses for band-selective and broadband inversion.

3.3. Broadband excitation of x magnetization with minimum phase error

Here we ask the question of whether the duration of broadband excitation pulses can be reduced using the COOP approach. In order to avoid phase errors in the resulting spectrum, a single pulse for broadband excitation of x magnetization is not allowed to create significant y components in the desired offset range. In contrast, the creation of relatively large y components $|M_y^{(j)}(T)|$ by the individual members of a cycle of COOP excitation pulses is acceptable, provided $|\overline{M}_y(T)|$ is small (and $\overline{M}_x(T)$ is large). This provides additional degrees of freedom in the optimization.

As a concrete example, we consider the optimal excitation of x magnetization with minimal phase errors in an offset range of ±20 kHz with a maximum rf amplitude of $\nu_{rf}^{max} = 17.5$ kHz [16–18] and a robustness with respect to variations of the rf amplitude of ±5%. For this problem, the duration of efficient optimal control based pulses could be reduced from 2 ms [16] to 500 μs [17] by generalizing the algorithm to take rf limit limits into account during the optimization. Subsequently, the pulse duration could be reduced even further to only 125 μs [18] by using a quality factor similar to Φ_c (Eq. (13)) for $N = 1$ that is better adapted to the problem of excitation with minimal phase errors than quality factors based on Φ_a (Eq. (6)).

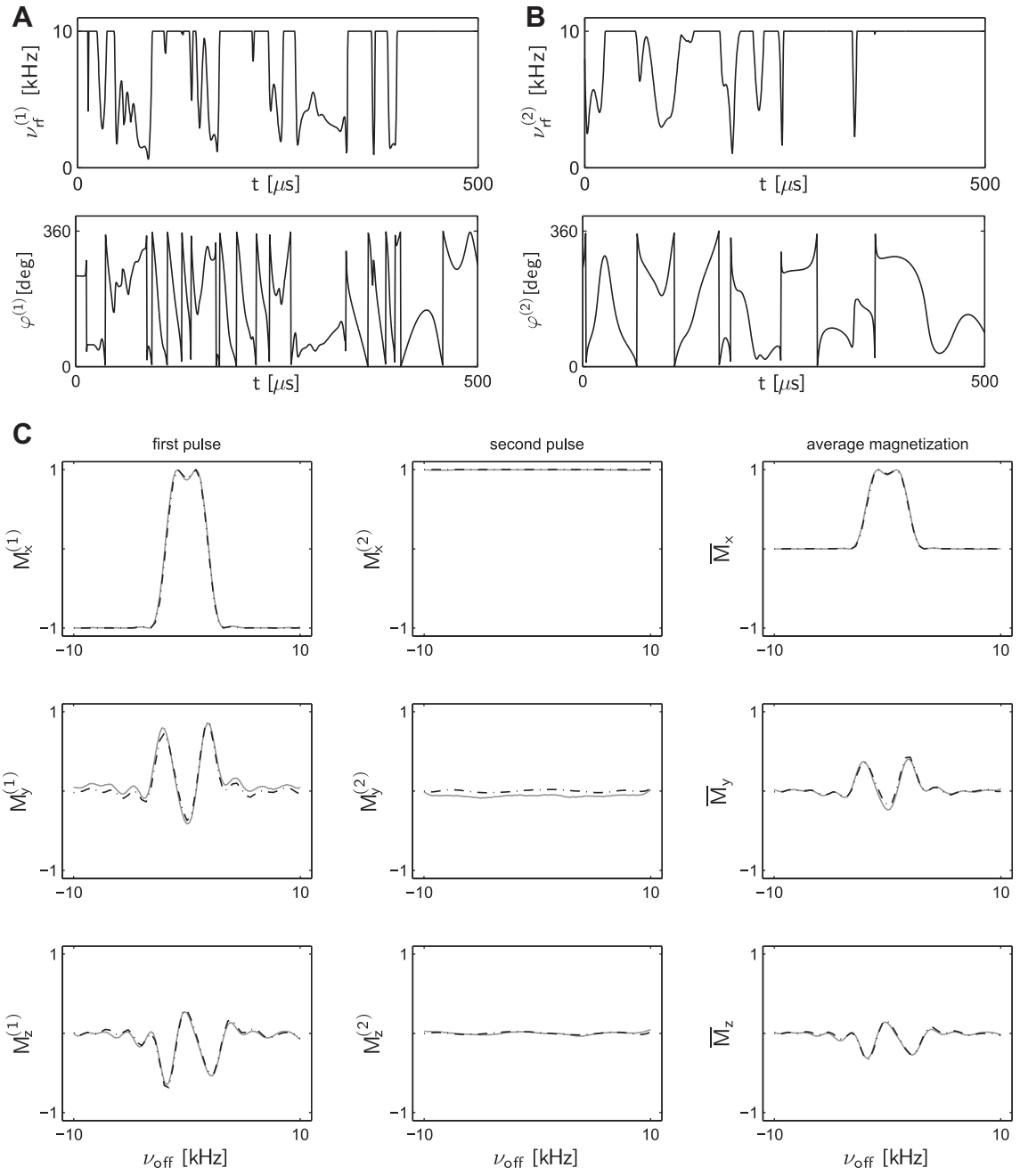

Fig. 3. Two conventional pulses that were independently optimized for band-selective and broadband excitation, respectively. The rf amplitudes $v_{rf}(t)$ and phases $\varphi(t)$ for each indivudual pulse are shown in A and B. Simulated (black, dash-dotted curves) and experimental (gray, solid curves) components of $\boldsymbol{M}^{(1)}(T)$, $\boldsymbol{M}^{(2)}(T)$ and $\overline{\boldsymbol{M}}(\boldsymbol{T})$ are shown in C.

For the same specifications, we optimized a single pulse ($N = 1$) and COOP cycles ($N > 1$) using the quality factor Φ_c (Eq. (13)). The numerically determined quality factor Φ_c (Eq. (13)) with $a = 1$ of the single 125 μs long pulse from [18] is $\Phi_c = 0.999852$. The gradient of the quality factor for the COOP pulse optimization can be efficiently approximated to first order using Eqs. (10) and (11), where $\boldsymbol{\lambda}^{(j)}(T)$ is given by Eq. (14). For example, for a three-step COOP cycle, a comparable quality factor ($\Phi_c = 0.999856$) can be achieved with a reduced duration of only 100 μs of each individual pulse (see supplementary material). Hence, in this case it is possible to reduce the duration of excitation pulses by an additional 20% without loss in pulse performance using the COOP approach. The x component of the excited average magnetization vector is about 0.99, and the phase error is less than 0.4° for the entire offset range of 40 kHz.

In order to explore the performance limit of even shorter pulses, we also optimized single and COOP pulses with a duration of $T = 50$ μs, which is only 3.5 times longer than the duration of a hard 90° pulse for an rf amplitude of 17.5 kHz. Fig. 4 shows the achieved quality factors for a single pulse ($N = 1$) and for COOP cycles with N between 2 and 6. The optimized pulses for $N = 1$, 2, and 3 are shown in Fig. 5. All pulses have constant amplitude, taking full advantage of the maximum allowed rf amplitude of $v_{rf}^{max} = 17.5$ kHz. The optimal single pulse ($N = 1$) shown in Fig. 5A is purely phase-alternating with phases ± $\pi/2$. This class of phase-alternating pulses implies the following symmetry relations

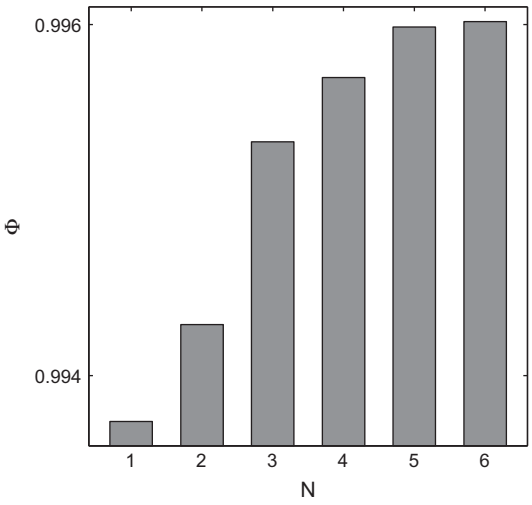

Fig. 4. Quality factor Φ for excitation of x magnetization with pulse durations of $T = 50$ μs as function of the number of COOP pulses N.

for the x and y components of the excited magnetization vectors at offsets $\pm\nu$ [2]:

$$M_x(\nu) = M_x(-\nu), \tag{16}$$
$$M_y(\nu) = -M_y(-\nu). \tag{17}$$

(In additon, $M_z(\nu) = M_z(-\nu)$, however this is not relevant here, as Φ_c has no explicit M_z dependence, c.f. Eq. (13).) The symmetry relations for the x and the y components of the final magnetization vectors match the symmetry of the problem: Maximum $M_x(\nu)$ is desired both for positive offsets (between 0 and 20 kHz) and for negative offsets (between 0 and −20 kHz), and, according to Eq. (16), a large $M_x(\nu)$ implies an equally large $M_x(-\nu)$. In addition, $|M_y|(\nu) \approx 0$ is desired both for positive and negative offsets, and, according to Eq. (17), a small $|M_y|(\nu)$ at frequency ν implies an equally small $|M_y|(-\nu)$.

In contrast to the case $N = 1$, the individual COOP pulses for $N = 2$ shown in Fig. 5B are not phase-alternating but have smooth phase modulations. However, the phase modulations are not independent but are related by phase inversion and an additional phase shift by π:

$$\varphi^{(2)}(t) = -\varphi^{(1)}(t) + \pi, \tag{18}$$

corresponding to a reflection of the phase around $\pi/2$. (In terms of the x and y components of the rf amplitudes, this relation corresponds to $\nu_x^{(2)} = -\nu_x^{(1)}$ and $\nu_y^{(2)} = \nu_y^{(1)}$.) Applying well known principles of pulse sequence analysis [2], it is straightforward to show that Eq. (18) implies the following symmetry relations between the transverse components of the excited magnetization vectors after the first and second pulse:

$$M_x^{(2)}(\nu) = M_x^{(1)}(-\nu), \tag{19}$$
$$M_y^{(2)}(\nu) = -M_y^{(1)}(-\nu) \tag{20}$$

(and in additon $M_z^{(2)}(\nu) = M_z^{(1)}(-\nu)$). As a direct consequence of Eqs. (19) and (20), the transverse components of the average magnetization vector after the two-step COOP cycle are related by

$$\overline{M}_x(\nu) = \overline{M}_x(-\nu), \tag{21}$$
$$\overline{M}_y(\nu) = -\overline{M}_y(-\nu). \tag{22}$$

which is analogous to the relations in Eqs. (16) and (17) for a single phase-alternating pulse and which matches the symmetry of the problem as discussed above. The symmetry relations for the average transverse magnetization components (Eqs. (21) and (22)) can always be realized if the N-step COOP cycle consists of symmetry-related pulse pairs (with phase relations corresponding to Eq. (18)) and/or phase-alternating pulses with phases $\pm\pi/2$. For example, the three-step COOP cycle consists of one symmetry-related pulse pair and one phase-alternating pulse (see Fig. 5C). For $N = 4$, 5, and 6, we always find two symmetry-related pulse pairs and an according number of phase-alternating pulses.

Fig. 6 shows the location of the individual and of the average magnetization vectors in the y-z plane after the three-step COOP cycle ($N = 3$) (c.f. Fig. 5C). The points denoted a, b, and c correspond to offsets of −20 kHz, 0 kHz and 20 kHz, respectively. Figs. 6B and C illustrate the symmetry relations of Eqs. (16), (17) and of Eqs. (21), (22). Relatively large y components of up to 40% are found for each individual pulse, illustrating the additional degrees of freedom gained by the COOP approach. However, the average magnetization

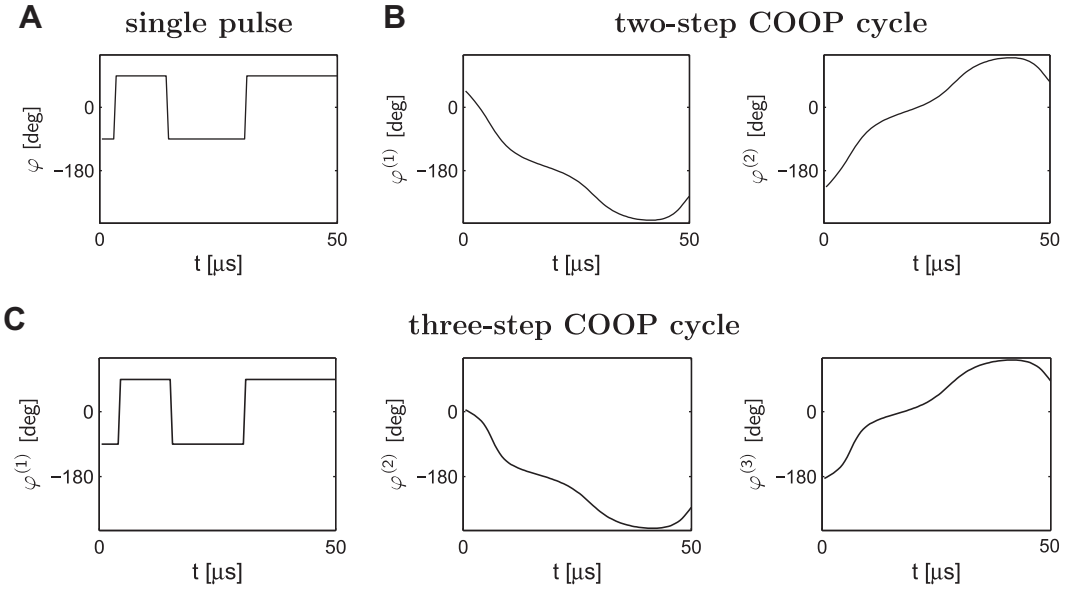

Fig. 5. Excitation pulses with minimized phase errors with a duration of $T = 50$ μs: (A) conventional single pulse, (B) two-step COOP cycle ($N = 2$), (C) three-step COOP cycle ($N = 3$). For both pulse pairs with "smooth" phase modulation in B and C, the individual pulses are symmetry-related by $\varphi^{(j+1)}(t) = -\varphi^{(j)}(t) - \pi$ which is equvalent to Eq. (18).

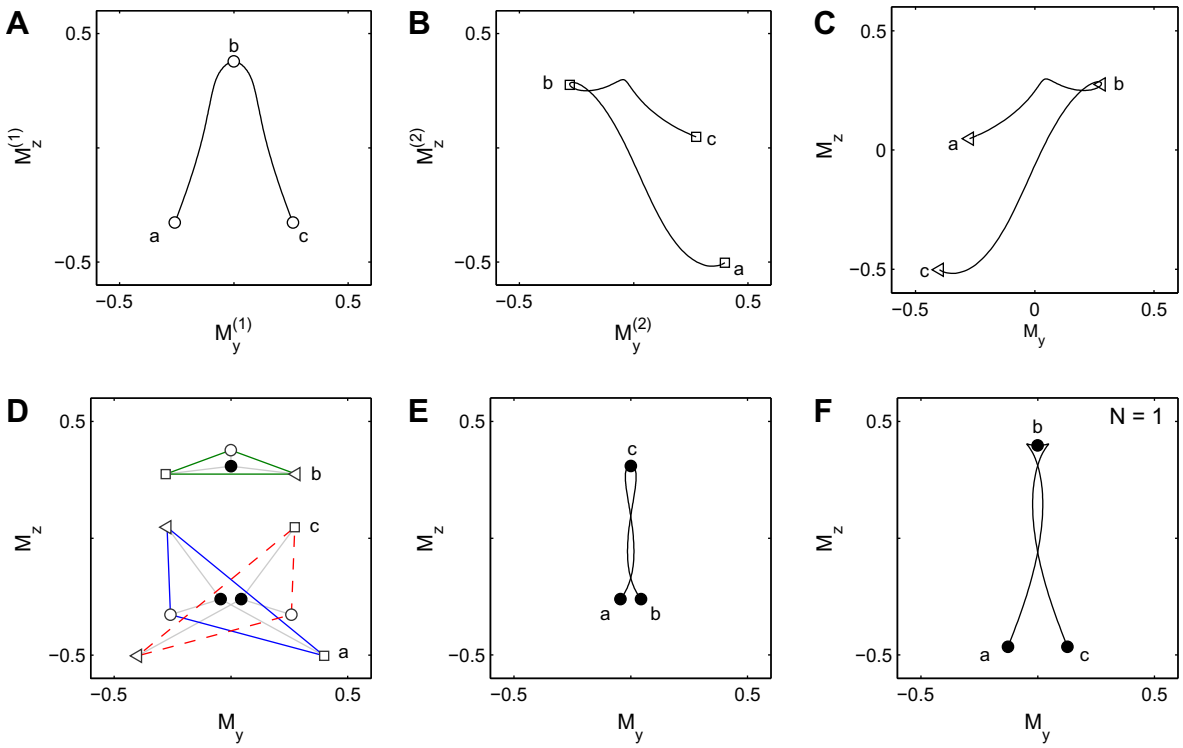

Fig. 6. In A–C, the individual offset-profiles for a three-step COOP cycle ($N = 3$) from Fig. 5C are shown. The final states of $M_y^{(j)}(T)$ and $M_z^{(j)}(T)$ within an offset frequency range of ±20 kHz are displayed, where in each subplot, the offsets −20 kHz, 0 kHz and 20 kHz are indicated by symbols (open circles, squares and triangles) denoted a, b and c, respectively. For these three offsets, the y and z components of $\boldsymbol{M}^{(1)}(T)$, $\boldsymbol{M}^{(2)}(T)$ and $\boldsymbol{M}^{(3)}(T)$ (open symbols) and of $\overline{\boldsymbol{M}}(\boldsymbol{T})$ (solid discs) are shown in D, illustrating the cancellation of phase errors. Subplot E shows the location of the average magnetization vector $\overline{\boldsymbol{M}}(\boldsymbol{T})$ for the entire offset range of ±20 kHz. For comparison, the location of the magnetization vector $\boldsymbol{M}(T)$ for the single, conventionally optimized pulse $N = 1$, c.f. Fig. 5A is shown in F.

vectors are located very close to the x-z plane as shown in Fig. 6E. In Fig. 6D, the corners of the triangles represent the locations of the magnetization vectors after the individual pulses and the centers of the triangles indicate the location of the average magnetization vectors for offsets −20 kHz (a), 0 kHz (b) and 20 kHz (c), illustrating the averaging process. For comparison, Fig. 6F also displays the location of the magnetization after the optimized single pulse pulse (c.f. Fig. 5A).

A good match is found between the simulated and experimental performance of the COOP pulses, as demonstrated in Fig. 7, where the x component and the phase of the average magnetization vector is shown for the optimized single pulse and for the COOP cycles with $N = 3$ and $N = 6$. For the single pulse, the excitation efficiency is below 92% for a large range of offsets, whereas for $N = 6$, the excitation efficiency approaches 95% for almost the entire offset range. At the same time, the largest phase error is reduced from about 8° to 5° at the extreme offsets and from about 3° to less than 1.3° for offsets between ±18 kHz.

In [18] we conjectured that for a single pulse a duration of 100 μs is a conservative lower limit for achieving better than 95% excitation efficiency and a phase error of no more than 4° in a relative bandwidth of $\Delta\nu_{off}/\nu_{rf}^{max} = 2.3$ and with rf tolerance of ±5%. With the COOP approach, we were able to push the lower limit on pulse length below 65 μs for $N = 6$ (data not shown).

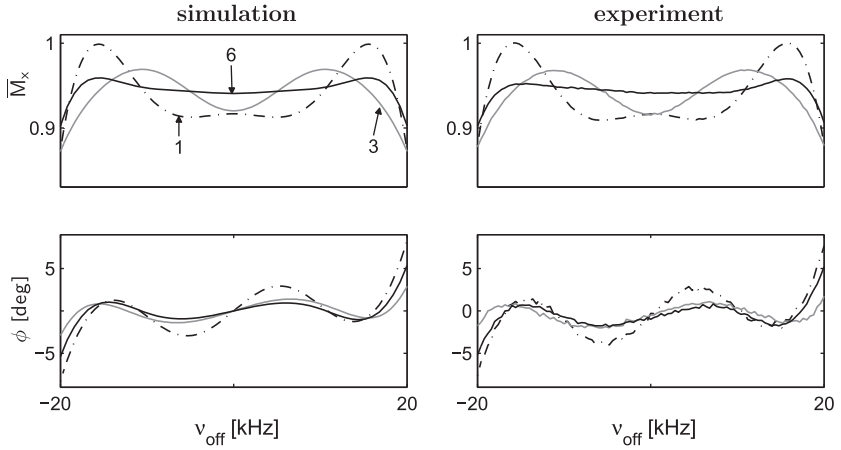

Fig. 7. Simulated and experimental offset-profiles for the average magnetization $\overline{M}_x(T)$ and the phase error $\pi(T)$ for a single pulse ($N = 1$, c.f. Fig. 5A) and COOP cycles with $N = 3$ (c.f. Fig. 5C) and $N = 6$.

3.4. Broadband excitation with linear offset dependence of phase

In the previous section the target was to create pulses with offset independent phase, i.e. pulses where no phase correction of first or higher order is necessary. As shown in [23], an even larger bandwidth can be achieved for so-called ICEBERG pulses that create transverse magnetization with a linear offset dependence of the phase. For example, for a simple rectangular 90° pulse, the resulting phase is almost linear for a large range of offsets and can be corrected by first-order phase correction. Fig. 8 shows the offset profile of the x component of $\overline{\boldsymbol{M}}_{\boldsymbol{x}}(\boldsymbol{T})$ magnetization and the residual phase error after first-order phase correction with 2.9°/kHz for a rectangular 14.29 μs 90° pulse, corresponding to an rf amplitude of ν_{rf} = 17.5 kHz. Over a range of ±50 kHz, the phase error is less than about 5°. However, for offset frequencies beyond ±30 kHz the excitation efficiency decreases rapidly (see Fig. 9).

We optimized a single pulse and a two-step COOP cycle (N = 2) with a duration of 60 μs each, a maximum rf amplitude 17.5 kHz, 5% rf inhomogeneity for a bandwidth of ±50 kHz allowing for the same first-order phase correction of 2.9°/kHz as for the simple rectangular pulse. Simulated and experimental results are displayed in Fig. 8. The performance of the optimized single pulse is significantly better than the simple rectangular pulse with larger transverse magnetization of more than 90% (except for offsets near −50 kHz where the efficiency drops to about 80%) compared to 45% and comparable phase errors. However, the performance of the optimized COOP pulses shows a significant further improvement with an excitation efficiency of more than than 95% and phase errors of less than 2.4° over the entire offset range of ±50 kHz.

3.5. COOP WET pulses

The final example demonstrating the power of the COOP approach is motivated by the WET (water suppression enhanced through T_1 effects) solvent suppression sequence [24,25]. In order to also suppress solvent signals in regions away from the center of the rf coil and therefore experiencing smaller rf amplitudes, pulses are required that act as broadband 90° pulses for the full rf amplitude but that do not excite the solvent signal in regions of the sample where the rf amplitude is significantly scaled down. One solution is based on a composite pulse, such as the

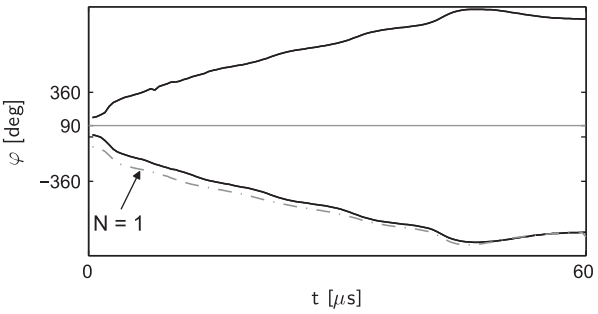

Fig. 9. A single (dashed-dotted gray curves) ICEBERG and a two-step (N = 2) COOP ICEBERG cycle (solid black curves). For the COOP pulse pair the symmetry relation from Eq. (18) is approximately fulfilled.

$90^\circ_x 90^\circ_y 90^\circ_{-x} 90^\circ_{-y}$ pulse [25,26], which is applied in every scan. However, in multi-scan experiments, improved performance was found if in three out of four scans a simple rectangular 90°_x pulse is used and in one out of four scans a simple rectangular 270°_{-x} pulse [25]. This set of four pulses (90°_x, 90°_x, 90°_x, 270°_{-x}), which are applied in successive scans, was derived in [25] based on linear response theory, which however is strictly valid only for flip angles approaching zero. In contrast, the COOP approach introduced here allows us to develop an optimized cycle of COOP pulses for this task, taking into account the full non-linear spins dynamics.

To illustrate this, we optimized COOP pulses with an excitation pattern [19] as a function of offset ν_{off} and rf scaling factor s that is adapted to the problem (see Fig. 10). For rf scaling factors in the range $0.95 \leqslant s \leqslant 1.05$, the goal is to excite x magnetization in an offset range of ±5 kHz with minimal phase error. For rf scaling factors in the range $0 \leqslant s \leqslant 0.6$, the goal is to minimize the transverse component $\overline{M}_\perp = (\overline{M}_x^2 + \overline{M}_y^2)^{1/2}$ of the average magnetization vector for a reduced range of offset (near the solvent resonance) of ±500 Hz. We assume initial z magnetization and a maximum nominal rf amplitude of $\nu_{rf}^{max} = 20$ kHz.

Figs. 10 and 11 show the performance of an optimized two-step COOP cycle (N = 2) with a duration T = 200 μs for each of the two individual COOP pulses. For comparison, we also show the performance of the composite pulse $90^\circ_x 90^\circ_y 90^\circ_{-x} 90^\circ_{-y}$ [26], of a sequence based on (90°_x, 90°_x, 90°_x, 270°_{-x}) [25] and an optimized individual pulse (N = 1).

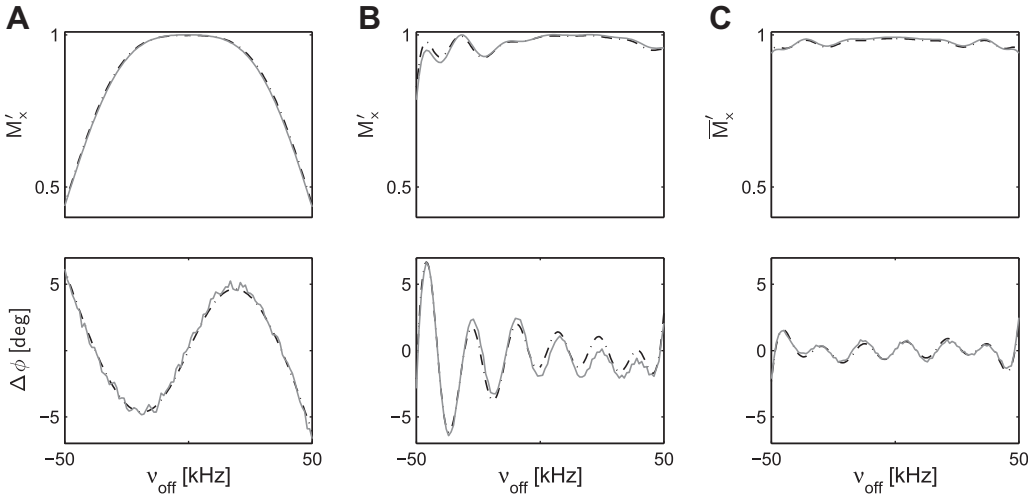

Fig. 8. Offset profiles for $\overline{M}'_x$ and phase deviation $\Delta\phi$ for a single rectangular pulse (A), an optimized individual ICEBERG pulse [23] with N = 1 (B, c.f. dash-dotted curve in Fig. 9) and a two-step COOP cycle (N = 2) (C, c.f. solid curves in Fig. 9). $\overline{M}'_x$ is the x-component of $\overline{\boldsymbol{M}}(\boldsymbol{T})$ and $\Delta\phi$ is the residual phase error after a first-order phase correction of 2.9°/kHz. Solid gray and dash-dotted black curves represent experimental and simulated data.

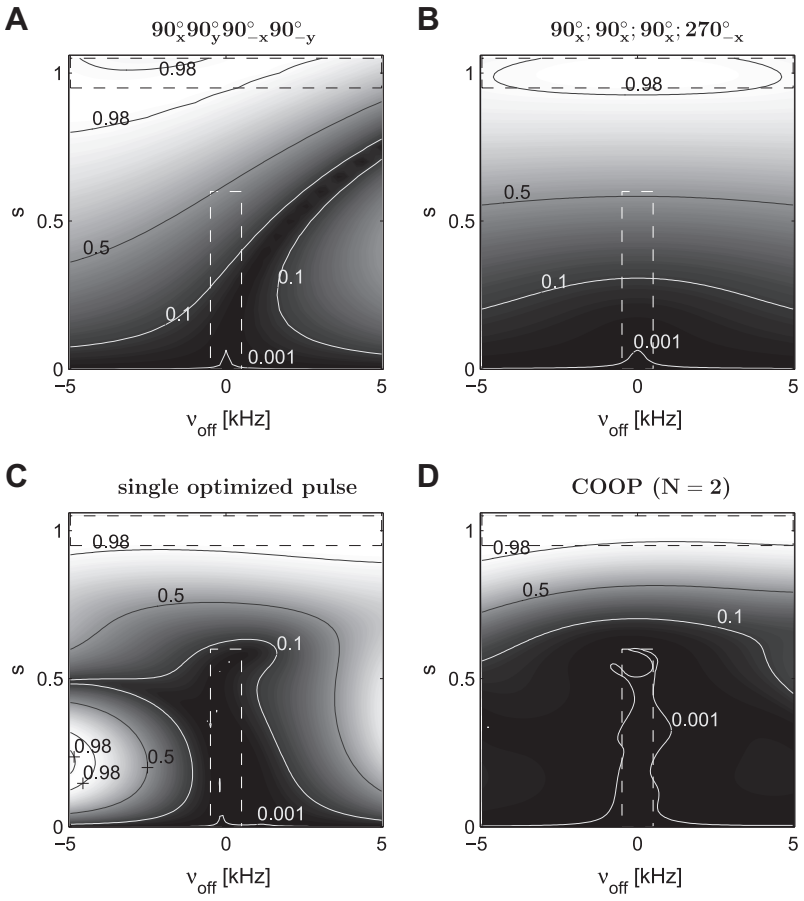

Fig. 10. Comparison of the average transverse magnetization as a function of offset ν_{off} and rf scaling s for a two-step cycle of COOP WET pulses (D, $N = 2$) with the $90^\circ_x 90^\circ_y 90^\circ_{-x} 90^\circ_{-y}$ composite pulse (A, [26]), the four-scan sequence based on $90^\circ_x; 90^\circ_x; 90^\circ_x; 270^\circ_{-x}$ (B, [25]) and an optimized individual pulse (C, $N = 1$). The areas for which optimal excitation and optimal suppression of transverse magnetization are desired are indicated by black and white dashed rectangles.

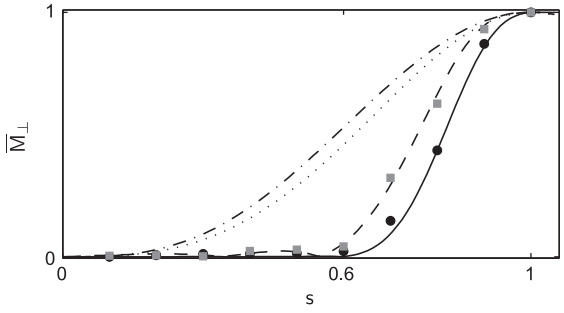

Fig. 11. Slices from Fig. 10A (dotted), B (dash-dotted), C (dashed) and D (solid curve) for the on-resonance case. The gray squares and black discs represent experimental data for the conventionally optimized pulse and the two-step COOP WET cycle from Fig. 10C and D, respectively.

4. Discussion and conclusion

Here, we introduced the concept of simultaneously optimized pulses that act in a cooperative way, compensating each others imperfections. Although for simplicity only examples involving uncoupled spins were considered, it is important to note that the COOP approach can also be applied to coupled spin systems. With the help of generalized optimal control based algorithms, such as the presented variant of the GRAPE (gradient ascent pulse engineering) algorithm, COOP pulses can be efficiently optimized.

Although the COOP approach is not limited to multi-scan experiments, here we focussed on applications where different members of a COOP cycle are used in different scans. In such multi-scan experiments, the COOP approach can be viewed as complementing and/or generalizing phase cycling [9–12] and difference spectroscopy. In conventional phase cycling, identical pulses are applied in each scan, up to an overall phase shift. In Section 3.1, the optimal COOP cycle also consisted of pulses that were identical up to an overall phase shift. Hence, it is possible to automatically generate phase cycles using the COOP approach. However, it is important to point out that here it was not possible to achieve the target of the optimization by considering coherence order pathways alone. Hence, the COOP solution relied on the simultaneous optimization of specific pulse shapes (saturation pulses) in combination with the resulting simple phase cycle. As demonstrated in Sections 3.2,3.3,3.4,3.5, COOP pulses are in general not simply related by overall phase shifts. In the presented COOP examples, a constant receiver phase was assumed. However, it is straightforward to lift this restriction by adding one additional control for the receiver phase for increased flexibility as in conventional phase cycles or in difference spectroscopy. In conventional difference spectroscopy, often different pulses are applied in successive scans. However, these pulses are typically either simple rectangular pulses or are optimized for each individual scan, not taking advantage of the full flexibility of the COOP approach introduced here. For example, this was illustrated in Section 3.5 for the problem of solvent suppression.

Optimal control based techniques for the efficient optimization of complex COOP pulses open new avenues for pulse sequence optimization. The goal of the presented examples was to illustrate the basic concept and to point out potential applications of COOP pulses. For example, in Section 3.5 it was demonstrated that the approach may be useful for water suppression techniques such as WET. However, for practical solvent suppression, it is necessary to adjust the design criteria for the optimized COOP pulses, which is beyond the scope of the present conceptual paper. It is also important to point out that the presented algorithm for the optimization of COOP pulses can be generalized in a straightforward way to include relaxation effects [13,21]. We hope that the presented COOP approach will find practical applications in NMR spectroscopy and imaging.

Pulse shapes of the discussed examples are available in electronic form in the supplementary material and at http://www.org.chemie.tu-muenchen.de/glaser/Downloads.html.

Acknowledgment

M. Braun thanks the Fonds der chemischen Industrie for a Chemiefonds stipend.

Appendix A. Supplementary material

Supplementary data associated with this article can be found, in the online version, at doi:10.1016/j.jmr.2010.08.013.

References

[1] R. Freeman, S.P. Kempsell, M.H. Levitt, Radiofrequency pulse sequences which compensate their own imperfections, J. Magn. Reson. 38 (1980) 453–479.
[2] M.H. Levitt, Composite pulses, Prog. Nucl. Magn. Reson. Spectrosc. 18 (1986) 61–122.
[3] M.H. Levitt, Composite pulses, in: D.M. Grant, R.K. Harris (Eds.), Encyclopedia of Nuclear Magnetic Resonance, Wiley, 1996.
[4] W.S. Warren, M.S. Silver, The art of pulse crafting: applications to magnetic resonance and laser spectroscopy, Adv. Magn. Reson. 12 (1988) 247–384.
[5] K. Kobzar, T.E. Skinner, N. Khaneja, S.J. Glaser, B. Luy, Exploring the limits of broadband excitation and inversion pulses, J. Magn. Reson. 170 (2004) 236–243.
[6] K. Kobzar, T.E. Skinner, N. Khaneja, S.J. Glaser, B. Luy, Exploring the limits of excitation and inversion pulses II. RF-power optimized pulses, J. Magn. Reson. 194 (2008) 58–66.
[7] J.L. Neves, B. Heitmann, T.O. Reiss, H.H.R. Schor, N. Khaneja, S.J. Glaser, Exploring the limits of polarization transfer efficiency in homonuclear three spin systems, J. Magn. Reson. 181 (2006) 126–134.
[8] A. Bryson Jr., Y.-C. Ho, Applied Optimal Control, Hemisphere, Washington, DC, 1975.
[9] J. Keeler, Understanding NMR Spectroscopy, Wiley, Chichester, 2005.
[10] G. Bodenhausen, H. Kogler, R.R. Ernst, Selection of coherence-transfer pathways in NMR pulse experiments, J. Magn. Reson. 58 (1984) 370–388.
[11] A.D. Bain, Coherence levels and coherence pathways in NMR, A simple way to design phase cycling procedures, J. Magn. Reson. 56 (1984) 418–427.
[12] M.H. Levitt, P.K. Madhu, C.E. Hughes, Cogwheel phase cycling, J. Magn. Reson. 155 (2002) 300–306.
[13] N. Khaneja, T. Reiss, C. Kehlet, T. Schulte-Herbrüggen, S.J. Glaser, Optimal control of coupled spin dynamics: design of NMR pulse sequences by gradient ascent algorithms, J. Magn. Reson. 172 (2005) 296–305.
[14] Z. Tošner, T. Vosegaard, C. Kehlet, N. Khaneja, S.J. Glaser, N.C. Nielsen, Optimal control in NMR spectroscopy: numerical implementation in SIMPSON, J. Magn. Reson. 197 (2009) 120–134.
[15] S. Conolly, D. Nishimura, A. Macovski, Optimal control solutions to the magnetic resonance selective excitation problem, IEEE Trans. Med. Imag. MI-5 (1986) 106115.
[16] T.E. Skinner, T.O. Reiss, B. Luy, N. Khaneja, S.J. Glaser, Application of optimal control theory to the design of broadband excitation pulses for high resolution NMR, J. Magn. Reson. 163 (2003) 8–15.
[17] T.E. Skinner, T.O. Reiss, B. Luy, N. Khaneja, S.J. Glaser, Reducing the duration of broadband excitation pulses using optimal control with limited rf amplitude, J. Magn. Reson. 167 (2004) 68–74.
[18] T.E. Skinner, T.O. Reiss, B. Luy, N. Khaneja, S.J. Glaser, Tailoring the optimal control cost function to a desired output: Application to minimizing phase errors in short broadband excitation pulses, J. Magn. Reson. 172 (2005) 17–23.
[19] K. Kobzar, B. Luy, N. Khaneja, S.J. Glaser, Pattern pulses: design of arbitrary excitation profiles as a function of pulse amplitude and offset, J. Magn. Reson. 173 (2005) 229–235.
[20] T.E. Skinner, K. Kobzar, B. Luy, R. Bendall, W. Bermel, N. Khaneja, S.J. Glaser, Optimal control design of constant amplitude phase-modulated pulses: Application to calibration-free broadband excitation, J. Magn. Reson. 179 (2006) 241–249.
[21] N.I. Gershenzon, K. Kobzar, B. Luy, S.J. Glaser, T.E. Skinner, Optimal control design of excitation pulses that accomodate relaxation, J. Magn. Reson. 188 (2007) 330–336.
[22] A. Wächter, L.T. Biegler, On the implementation of a primal-dual interior point filter line search algorithm for large-scale nonlinear programming, Math. Program. Ser. A 106 (2006) 25–57.
[23] N.I. Gershenzon, T.E. Skinner, B. Brutscher, N. Khaneja, M. Nimbalkar, B. Luy, S.J. Glaser, Linear phase slope in pulse design: application to coherence transfer, J. Magn. Reson. 192 (2008) 335–343.
[24] R.J. Ogg, P.B. Kingsley, J.S. Taylor, WET a T_1- and B_1-insensitive water-suppression method for in vivo localized ^{1}H NMR spectroscopy, J. Magn. Reson. B 104 (1994) 1–10.
[25] S. Zhang, X. Yang, D.G. Gorenstein, Enhanced suppression of residual water in a "270" WET sequence, J. Magn. Reson. 143 (2000) 382–386.
[26] A. Bax, A spatially selective composite 90° radiofrequencey pulse, J. Magn. Reson. 64 (1985) 142–145.